# THE INFLUENCE OF THE HEAT TREATMENT OVER THE MECHANICAL BEHAVIOR OF STEELS USED FOR ALTERNATOR SHAFTS

Brandusa GHIBAN[1], Valeriu RUCAI[2], Nicolae NĂVODARIU[3], Vicențiu SĂCELEANU[4], Dragoș-Teodor BRAN[5]

*The present paper analyzes properties such as the hardness, the tensile and toughness begaviour and the microstructure for multiple bars of C40 and C45 steel used for shafts in alternators. The materials have been manufactured by rolling processes, followed by normalization treatments or forging processes followed by normalization treatments. Heat treatments are performed on steels to produce different microstructural phases that affect the mechanical properties. Microstructural changes during austenite decomposition depend on the transformation temperature region and cooling rate. Over the years, many experimental studies have been performed to reveal the microstructural changes during isothermal holding or continuous cooling of austenite for various kinds of steels. The isothermal transformation (IT) diagram, which is also called the time-temperature-transformation (TTT) diagram, and the continuous cooling transformation (CCT) diagram have been developed to graphically characterize the decomposition transformation as a function of time and temperature. However, when these diagrams are based on experimental measurements, several limitations are present. Each diagram is limited because the temperatures at which specific transformations occur can vary due to several factors, such as: the chemical composition of steel, the solid solution condition in the austenite prior to cooling and transformation, the presence of precipitates in austenite, the prior austenite grain size, and the applied stresses during the transformation.*

## 1. Introduction

Heat treatments are performed on steels to produce different microstructural phases that affect the mechanical properties. Microstructural changes during austenite decomposition depend on the transformation temperature

[1] Professor, Metallic Materials and Physical Metallurgy Department, Faculty of Materials Science and Engineering, University POLITEHNICA of Bucharest, Romania, e-mail: ghibanbrandusa@yahoo.com
[2] Lecturer, Faculty of Materials Science and Engineering, University POLITEHNICA Bucharest,
[3] PhD student, Metallic Materials and Physical Metallurgy Department, Faculty of Materials Science and Engineering, University POLITEHNICA of Bucharest, Romania, e-mail: nicolae.navodariu@volvo.com
[4] Professor, Faculty of Medicine, University *Lucian Blaga*, Sibiu
[5] PhD Student, Metallic Materials and Physical Metallurgy Department, Faculty of Materials Science and Engineering, University POLITEHNICA of Bucharest, Romania, e-mail: dragos.bran@yahoo.com

region and cooling rate. Over the years, many experimental studies have been performed to reveal the microstructural changes during isothermal holding or continuous cooling of austenite for various kinds of steels. The isothermal transformation (IT) diagram, which is also called the time-temperature-transformation (TTT) diagram, and the continuous cooling transformation (CCT) diagram have been developed to graphically characterize the decomposition transformation as a function of time and temperature. However, when these diagrams are based on experimental measurements, several limitations are present. Each diagram is limited because the temperatures at which specific transformations occur can vary due to several factors, such as: the chemical composition of steel, the solid solution condition in the austenite prior to cooling and transformation, the presence of precipitates in austenite, the prior austenite grain size, and the applied stresses during the transformation.

The present paper analyzes properties such as the hardness, the tensile and toughness begaviour and the microstructure for multiple bars of C40 and C45 steel used for shafts in alternators. The materials have been manufactured by rolling processes, followed by normalization treatments or forging processes followed by normalization treatments.

## 2. Theoretical considerations

Plain carbon steels have a limited hardenability. Hardenability is the depth or maximum diameter where a 50% martensitic microstructure can be achieved; it is expressed as an ideal diameter and can be calculated for any alloy content using ASTM A255-10 ‘Standard Test Methods for Determining the Hardenability of Steel’. The use of alloying elements such as Ni, Mo, Mn, and Cr increases the hardenability of steel. By increasing the hardenability of an alloy, greater case depths can be achieved. In addition to alloying to improve hardenability, microalloy additions of Nb, V, Al, and Ti can be used to form carbides and nitrides that retard grain growth during the austenitizing process and improve the tempering response of the material, which may improve the mechanical performance of the steel. Transformation of austenite is plotted against temperature vs time on a logarithm scale to obtain the TTT diagram. TTT diagrams give the kinetics of isothermal transformations and the diagrams are either S or C shaped. At higher under cooling or lower temperatures, finer pearlite structure are formed. At the nose of the TTT diagram, a very fine pearlite structure is formed.

The CCT diagram depends on the composition of the steel, the nature of cooling, austenite grain size, extent of austenite homogenising and also the austenitising temperature and time. Similar to TTT diagrams, there are different regions for different transformations (i.e. cementite/ferrite, pearlite, bainite and martensite). There are transformation start and transformation finish lines and

isopercentage lines. However, depending on the factors mentioned earlier, some of the transformation may be absent or some transformations may be incomplete. In general for ferrite, pearlite and bainite, the transformation start and finish temperature moves towards lower temperatures and transformation times towards higher timing in comparison to isothermal transformation, transformation curves moves down and right. The bainite reaction can be sufficiently retarded such that transformation takes shelter completely under the pearlitic transformation in case of the eutectoid plain-carbon steel and therefore the bainite region vanishes. However, in other steels it may be partially sheltered. Therefore, the bainitic region is observed in non-eutectoid plain-carbon or alloy steels.

The nose of the C curves moves to a lower temperature and longer time. So the actual critical cooling rate required to avoid diffusional transformation during continuous cooling is less than as prescribed by TTT diagram and the hardenability is higher than that predicted by TTT. Ms temperature is unaffected by the conventional cooling rate.It is reported that the micro-hardness of martensite is only influenced by the cooling rate from 700 °C [1].

### 2.1 Heat treatment of C40 steel

Gür and Cam [2] used 5 mm thick disk shaped specimens cut perpendicular to the rolling direction of the hot-rolled 30 mm diameter SAE 1040. Following the austenitization at 850 °C for 30 min, the SAE 1040 specimens were heat treated according to the procedures given in Table 1.

Tayanç et al. [3] used the as-received SAE 1040 steel material that came in the form of hot-rolled bars, approximately 5.1 mm in diameter for their study.

*Table 1*

**Heat treatment of the SAE 1040 specimens following austenitization at 850°C for 30min, and corresponding microstructures [2]**

| Heat Treatment | Microstructure |
|---|---|
| Water quenching (20°C) | Martensite |
| Water quenched and subsequent tempering at 600 °C for 120 mins | Tempered martensite |
| Isothermal heat treatment in molten salt bath at 600 °C for 10 mins and water quenched | Pearlite–ferrite (fine) |
| Isothermal heat treatment in molten salt bath at 680 °C for 60 mins and water quenched | Pearlite–ferrite (coarse) |

They performed two-phase annealing (intercritically annealing) on the SAE 1040 steels which were held in the furnace at 745, 760, 775, and 790 °C for 30 min, then the specimens were quenched directly into water to obtain dual-phase (martensite-plus-ferrite) structure. After heat treatment, cross-sections of samples were polished, etched with 5% nital, and observed under light microscope to reveal the morphology of the phases. The volume fraction of

martensite of the SAE 1040 steel was determined using the point counting method. Pan et al. [6] studied the effect of electric current pulse (ECP) treatment on AISI 1045, producing, engineering stress-strain curves of specimens before and after electric current pulse (ECP) treatment.

### 2.2 Heat treatment of C45 steel

Zhang et al. [4] examined the influence of the microstructure on 1045 steel using five different heat treatment conditions. Table 2 shows the influence of various heat treatment conditions on the 1045 steel specimens and the corresponding microstructures.

*Table 2*

**Various heat treatment conditions of 1045 steel and the corresponding microstructures [4]**

| Heat Treatment | Microstructure | Hardness (HRC) |
|---|---|---|
| 860 °C quenched | Martensite | 55-57 |
| 860 °C quenched + 250 °C tempered | Tempered martensite | 43-46 |
| 860 °C quenched + 400 °C tempered | Tempered troostite | 34-36 |
| 860 °C quenched + 600 °C tempered | Tempered sorbite | 27-29 |
| 840 °C annealed | Ferrite and pearlite | 8-10 |

Wehner and Fatemi [5] evaluated the uniaxial mechanical properties of a typical automotive steel, SAE 1045 which was hardened to 55 HRC from 25 HRC. The microstructure of the hardened material consisted of martensite along with austenite and bainite. The surface hardness variation was checked by Wehner and Fatemi on eight different specimens and ranged from 51.7 HRC to 56.25 HRC with an average of 54.3 HRC. In addition to this, two specimens were sectioned across their 12.7 mm diameter to check the variation in hardness over the cross section. At 0.09 mm from the edge of the specimen the hardness was 55 HRC, which gradually decreased to 51 HRC at the centre of the specimen. The higher hardness near the surface was probably the result of some additional carbon from the atmosphere during the heat treatment process, which included tempering at 176.67 °C for one hour.

The results showed that ECP treatment can improve the tensile strength when compared to the as-quenched condition but does not increase ductility, which was far less than the tempered condition. Castro et al. [7] evaluated the detailed characterization of the heat treatment performed on SAE 1045 steel. After initial characterization in the as-received conditions, discs were heat-treated using the following method: austenitization at 850 °C for 30 min and quenching in water, tempering at 100 °C and 300 °C for 30 min and cooling in air. The hardness and the microstructure of the SAE 1045 steels in the (a) as-received, (b) quenched and tempered at 100 °C and (c) quenched and tempered at 300 °C conditions are shown in Table 3.

*Table 3*

**Various heat treatment conditions on the SAE 1045 steel specimens and the corresponding hardness and microstructures [7]**

| Heat Treatment | Microstructure | Hardness (HRC) |
|---|---|---|
| As-received | Ferrite surrounded colonies of lamellae pearlite | 11 |
| 850 °C austenitization for 30 mins, then water quenched followed by tempering at 100 °C for 30 mins and air cooling | Tempered martensite with some bainite | 61 |
| 850 °C austenitization for 30 mins, then water quenched followed by tempering at 300 °C for 30 mins and air cooling | Coarser tempered martensite | 52 |

## Experimental research

Two shafts have been used for this experimental research. One shaft was manufactured from C40 steel, with a diameter of 200mm, rolled and normalized, and the other shaft was manufactured from C45 steel, also hot rolled and normalized, with a diameter of 270mm. We can consider that the two shafts have close dimensions from the heat treatment point of view and the main difference between them would be represented by the different chemical composition of the steel.

In order to test these shafts, multiple analysis have been performed: the hardness, microstructure, the chemical composition, tensile tests and Charpy tests. For the extraction of samples for the above-mentioned tests, the EDM method has been used and the material has been initially cut at 130mm from one end, along the radial direction, to extract a disc with a thickness of 10mm. The cut section can is displayed in Fig. 1. The extracted10mm thick disc was used for the hardness measurement and microstructure alanalysis.

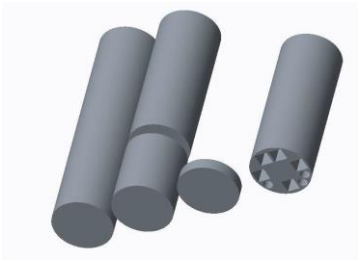

Fig.1. Cut section for metallurgical analysis

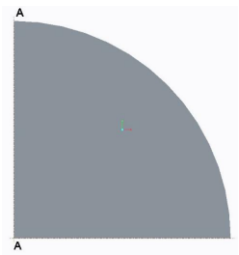


Fig. 2. Hardness measurement along the line A-A

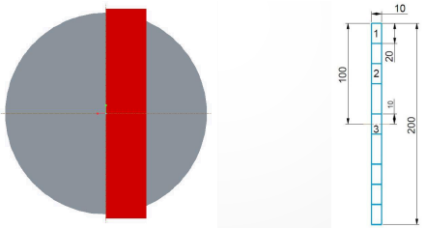


Fig. 5. Specimen extraction location for optical microstructure analysis.

### 2.3 Hardness results

The hardness measurement of the C40 sample was measured along the radial direction at a load of 20kg, using the diamond pyramid indenter. The section representation of the sample is presented in Fig. 2.
On the section A-A, presented in Fig. 9, 26 measurements have been taken, from the surface of the material, to the core for the C40 sample and 34 measurements have been taken for the C45 sample, in a similar manner and direction.
The results of the hardness test for the C40 sample are presented in Fig. 3. The average hardness is 181 HV20 and the standard deviation is 3 according to the test data.

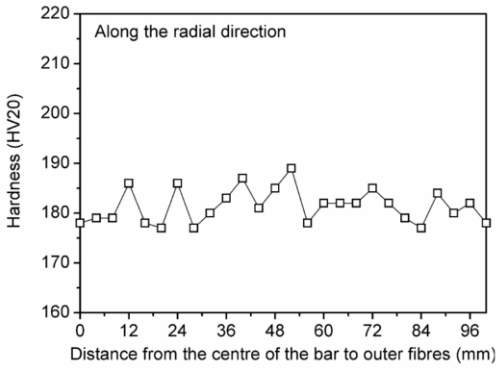


Fig. 3. Hardness results for C40 steel sample

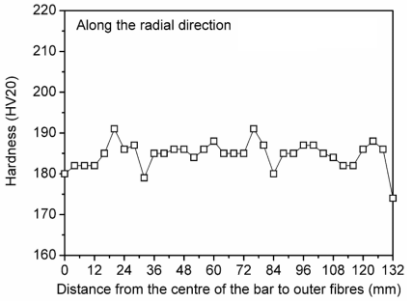


Fig. 4. Hardness results for C45 steel sample

In a similar manner, the hardness has been tested also for our C45 sample. The results of the hardness test for the C45 sample are presented in Fig. 4. The average hardness is 185 HV20 and the standard deviation is 3 according to the test data.

The hardness results are very similar but it is worth mentioning that the C45 sample has had a slightly higher hardness. Nevertheless, the number of analysis is large enough for a good statistical population and thus, along with the low standard deviation, we can be certain of the presented values. The main difference in these materials, the chemical composition, will be discussed in the next chapter.

### Chemical composition

The chemical composition of the C40 and C45 samples have been analysed using the spark emission testing. Table 4 presents the chemical composition of C40 and C45 steel according to the British Standard BS EN10083-2 :2006 [8].

For each of the samples used in this research, a number of 10 measurements has been performed in 10 different locations. Table 5 presents the mean result of the test data and also the standard deviation for both materials.

*Table 4.*

**Chemical composition of C40 and C45 according to BS EN10083-2:2006**

| sample | | C | Si | Mn | P | S | Ni | Cr | Mo | Fe | Cr+Mo+Ni |
|---|---|---|---|---|---|---|---|---|---|---|---|
| **C40** | min. | 0.37 | --- | 0.50 | --- | --- | --- | --- | --- | Rem. | --- |
| | Max. | 0.44 | 0.40 | 0.80 | 0.045 | 0.045 | 0.40 | 0.40 | 0.10 | | 0.63 |
| **C45** | min. | 0.42 | --- | 0.50 | --- | --- | --- | --- | --- | Rem. | --- |
| | Max. | 0.5 | 0.40 | 0.80 | 0.045 | 0.045 | 0.40 | 0.40 | 0.10 | | 0.63 |

*Table 5.*

**The results of the 10 measurements – mean and standard deviation**

| | | C | Si | Mn | P | S | Ni | Cr | Mo | Fe | Cr+Mo +Ni |
|---|---|---|---|---|---|---|---|---|---|---|---|
| **C40** | mean | 0.430 | 0.300 | 0.760 | 0.027 | 0.004 | 0.041 | 0.006 | 0.005 | 98.20 | 0.052 |
| | St. dev | 0.008 | 0.006 | 0.017 | 0.001 | 0.001 | 0.006 | 0.001 | --- | 0.05 | --- |
| **C45** | mean | 0.461 | 0.300 | 0.736 | 0.022 | 0.026 | 0.033 | 0.169 | 0.007 | 97.96 | 0.209 |
| | St. dev | 0.015 | 0.007 | 0.009 | 0.001 | 0.008 | 0.003 | 0.004 | 0.004 | 0.05 | --- |

The chemical composition shows a higher carbon content in C45 steel than in C40, as expected and the other elements have a similar value. Between the two used materials, another notable difference is given by other alloying elements such as the total of Cr, Mo and Ni.

### 2.4 Microstructure analysis

In order to study the microstructure analysis for the C40 and C45 samples, the 10mm discs mentioned in Fig. 1 have been cut into 10mm x 200mm long samples for the C40 shaft and 10 mm x 270 mm for the C45 shaft. For reference, please consult Fig. 5. Three zones have been identified on the obtained cut part: the outer fibers, the inner fibers and the core. Each zone has been designated a length of 20mm.The microstructure analysis was performed on all three locations: outer fibers, inner fibers and the core of the shafts. Fig. 6 presents the optical microstructure from the outer fibre of the shaft made from C40 Steel. The images were taken at 1mm below the top location of the sample. Also, the perlite volume is marked on the image as $V_F$ and the perlite volume is marked $V_P$ on the image.

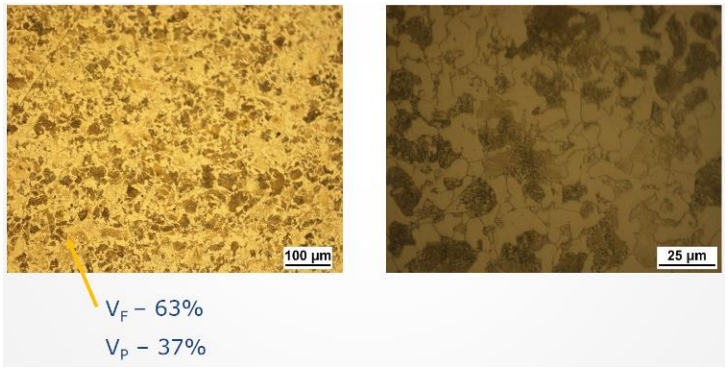


Fig. 6. Microstructure at the top of the outer fibers for C40 sample

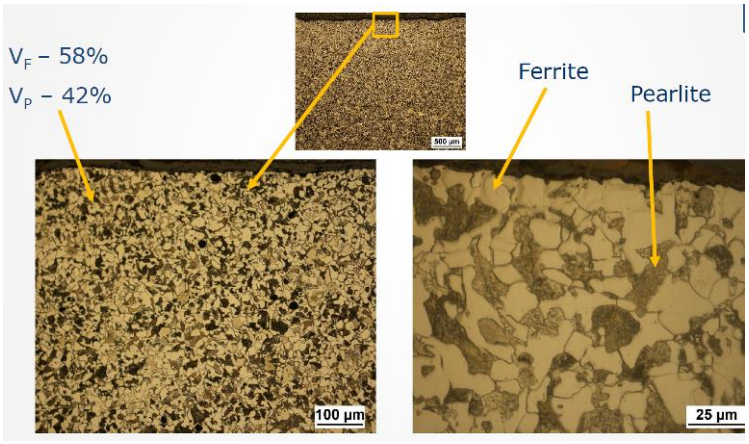


Fig. 7. Microstructure at the top of the outer fibers for C40 sample

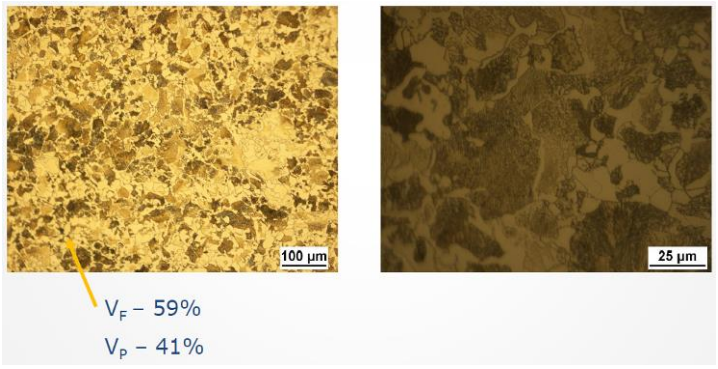


Fig. 8. Microstructure at the center of the inner fibers for C40 sample

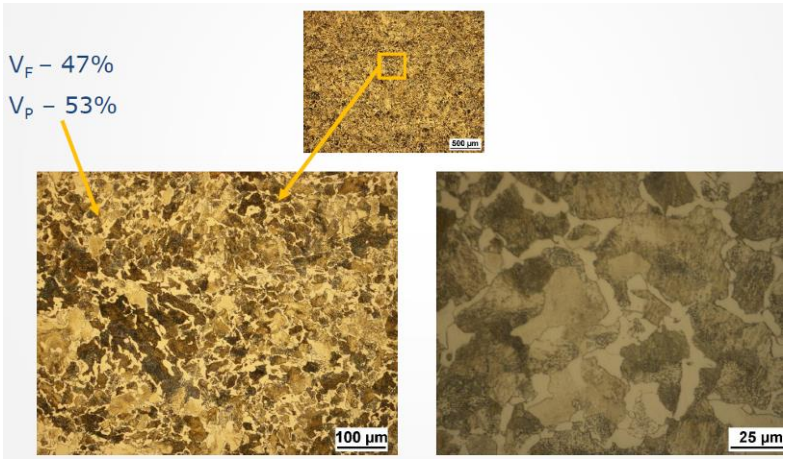


Fig. 9. Microstructure at the center of the inner fibers for C45 sample

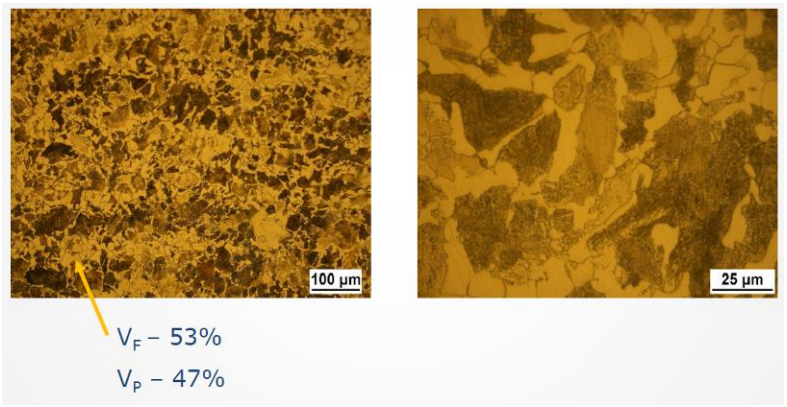


Fig. 10. Microstructure at the center of the core for C40 sample

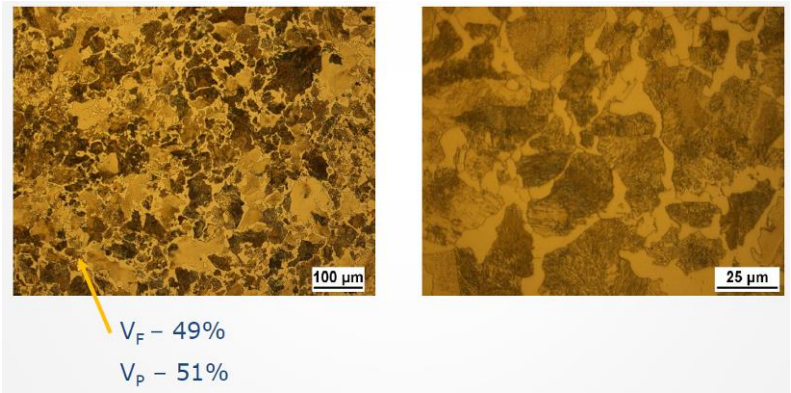


Fig. 11. Microstructure at the center of the core for C45 sample

Fig. 7 presents the optical microstructure from the outer fibre of the shaft made from C45 Steel. The images were taken at 1mm below the top location of

the sample. The volumes of ferrite and perlite have been obtained using software analysis. The inner fibers have also been analyzed for C40 and C45 samples. Fig. 8 presents the images taken from the center location of the sample for the C40 sample Fig. 9 presents the images taken at the center of the sample for the C45 sample. The core has been analyzed for C40 and C45 samples. Fig. 10 presents the images taken from the center location of the sample for the C40 sample Fig. 11 presents the images taken at the center of the sample for the C45 sample. It is evident from the microstructure analysis that the microstructure of all samples contains perlite colonies in a matrix of ferrite. The microstructure of the shafts is composed of randomly distributed ferrite and pearlite structure at other locations. The difference in the surface microstructure of the shaft can only be due to the machining. The significant heat input during the machining operation might have caused grain growth near the surface but some recrystallization (dynamic) right near the surface may have also taken place due to the plastic deformation from the machining process. The grains are random oriented. The microstructure is similar to the one reported by Ranc et al. [2] and Okayasu and Wang [3].

### 2.5 Mechanical trials: Tensile testing and Charpy testing

In order to understand the material behavior of the two shafts made from C40 and C45, tensile testing has been performed. For the first shaft, made from C40, 3 samples have been tested and from the C45 bar only 2 samples have been tested because the results were consistent. The tensile results are presented in the charts from Figs. 12 and Figure 13 for C40 and C45 respectively and the values are given in Table 6 below.

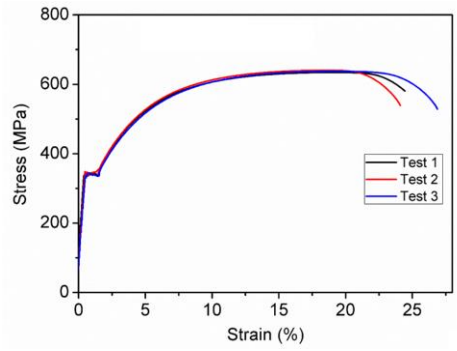


Fig. 12. Tensile results for C40 sample

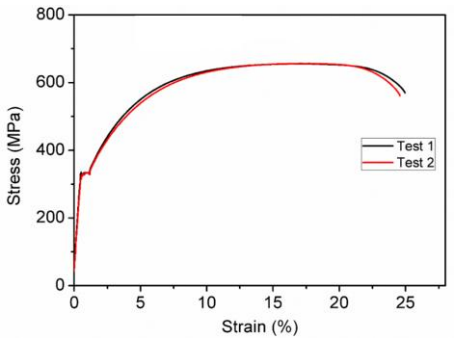


Fig. 13. Tensile results for C45 sample

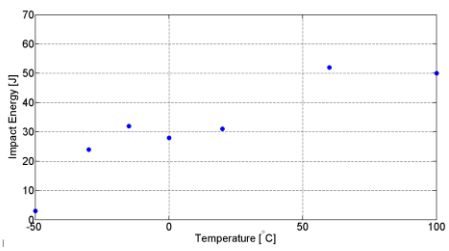


Fig. 14. Charpy results for C40 sample

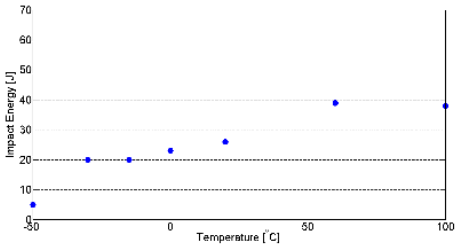


Fig. 15. Charpy results for C45 sample

It is clear that for the two materials, the yield strength is similar but when it comes to the ultimate tensile strength, C4 has slightly higher values.
The final tests that have been performed for this study were the Charpy test, using U-notch specimens, and an arrangement in accordance with the ASTM standard E23 [9]. For each material, 7 samples have been cut out and tested. The results are presented in Table 7 and also represented as a scatter chart in Fig. 14 for C40 and Fig. 15 for C45. The results have been measured with a classic analogical dial gauge and also with a load cell

*Table 6.*

**Tensile results for C40 and C45**

| | **C40** | | **C45** | |
|---|---|---|---|---|
| | **YS (MPa)** | **UTS (MPa)** | **YS (MPa)** | **UTS (MPa)** |
| **Test 1** | 339.56 | 634.8 | 339.57 | 655.75 |
| **Test 2** | 340.18 | 640.81 | 329.23 | 656.57 |
| **Test 3** | 352.11 | 637.9 | --- | --- |
| **Average** | 343.95 | 637.8367 | 334.4 | 656.16 |

*Table 7.*

**Impact energy results for C40 and C45**

| | | C40 | | C45 | |
|---|---|---|---|---|---|
| Test no. | Temp. (°C) | Dial gauge reading (J) | Load Cell Reading (J) | Dial gauge reading (J) | Load Cell Reading (J) |
| 1 | -50 | 3 | 2.13 | 5 | 4.11 |
| 2 | -30 | 24 | 22.52 | 20 | 19.27 |
| 3 | -15 | 32 | 26.16 | 20 | 20.14 |
| 4 | 0 | 28 | 27.13 | 23 | 21.94 |
| 5 | 20 | 31 | 31.27 | 26 | 25.72 |
| 6 | 60 | 52 | 46.62 | 39 | 36.43 |
| 7 | 100 | 50 | 48.31 | 38 | 36.52 |

The first sample, C40 had lower results for very low temperatures but the general behavior was better for this alloy than in the case of C45.

## 3. Conclusions

This study has analyzed 2 shaft materials used in electrical generators. One shaft was made from C40 and the other one was made from C45 steel, as per BS EN10083-2:2006. The analyzed materials have been previously subjected to heat treatments. First, the materials were hot rolled and then the materials have been normalized. The bars have been cut into smaller samples using the EDM cutting machine. The tests that were performed were: hardness testing, microstructural analysis, tensile testing and Charpy testing. The microstructural analysis was performed in 3 locations: the outer fibers, the inner fibers and the core of both materials. The results were close for the two materials, C40 and C45 for all the samples but is notable to state that for hardness, C45 had slightly better results and for impact testing, C40 obtained better results than C40. Both alloy can be easily manufactured and since they have similar properties, they can be both used to manufacturing the shafts of electrical machines such as generators or motors, as indicated by the standard BS EN 10083:2.

## R E F E R E N C E S

[1]. Gao, K., et al., Numerical and experimental analysis of 3D spot induction hardening of AISI 1045 steel. Journal of Materials Processing Technology, 2014. **214**(11): p. 2425-2433.

[2]. Gür, C.H. and I. Cam, Comparison of magnetic Barkhausen noise and ultrasonic velocity measurements for microstructure evaluation of SAE 1040 and SAE 4140 steels. Materials Characterization, 2007. **58**(5): p. 447-454.

[3]. Tayanc, M., A. Aytac, and A. Bayram, The effect of carbon content on fatigue strength of dual-phase steels. Materials & design, 2007. **28**(6): p. 1827-1835.

[4]. Zhang, N., et al., Effect of the substrate state on the microstructure and tribological properties of sulphide layer on 1045 steel. Applied surface science, 2000. **161**(1): p. 170-177.

[5]. Wehner, T. and A. Fatemi, Effects of mean stress on fatigue behaviour of a hardened carbon steel. International Journal of Fatigue, 1991. **13**(3): p. 241-248.

[6]. Pan, L., W. He, and B. Gu, Effects of electric current pulses on mechanical properties and microstructures of as-quenched medium carbon steel. Materials Science and Engineering: A, 2016. **662**: p. 404-411.

[7]. Castro, V.V., et al., Lubricated sliding wear of SAE 1045 and SAE 52100 steel against alumina in the presence of biodiesel, diesel and a 50: 50 blend of those fuels. Wear, 2016. **368**: p. 267-277.

[8]. BS EN10083-2 :2006

[9]. Rac et al, Study of thermal effects associated with crack propagation during very high cycle fatigue tests, Acta Materialia 56 (2008) 4012–4021

[10]. Okayasu and Wang, Etching technique for revelation of plastic deformation zone in low carbon steel, Materials Science and Technology, 21:5, 530- 538, DOI: 10.1179/174328405X36511

[11]. Gheorghe, D., Pop D., et al., Microstructure development in titanium and its alloys used for medical applications, U.P.B. Sci. Bull., Series B, 2019, 81(1): 243-258.

[12]. Antoniac I; Sinescu C; Antoniac A; Adhesion aspects in biomaterials and medical devices, Journal of Adhesion Science and Technology, 2016, 30(16):1711-1715.

[13]. Bita AI; Stan GE; Niculescu M; Ciuca I; Vasile E; Antoniac I; Adhesion evaluation of different bioceramic coatings on Mg-Ca alloys for biomedical applications, JOURNAL OF ADHESION SCIENCE AND TECHNOLOGY, Volume 30, Issue 18, Pages 1968-1983, 2016

[14]. Ionescu R; Mardare M; Dorobantu A; Vermesan S; Marinescu E; Saban R; Antoniac IV; Ciocan DN; Ceausu M; Correlation Between Materials, Design and Clinical Issues in the Case of Associated Use of Different Stainless Steels as Implant Materials, KEY ENGINEERING MATERIALS, Volume 583, Pages 41-44, 2014

[15]. Ionescu R; Cristescu I; Dinu M; Saban R; Antoniac I; Vilcioiu D; Clinical, Biomechanical and Biomaterials Approach in the Case of Fracture Repair Using Different Systems Type Plate-Screw, KEY ENGINEERING MATERIALS, Volume 583, Pages 150-154, 2014

[16]. Buzatu M; Geanta V; Stefanoiu R; Butu M; Petrescu MI; Buzatu M; Antoniac IV; Iacob G; Niculescu F; Ghica, SI; Moldovan H; Investigations into Ti-15Mo-W Alloys Developed for Medical Applications, MATERIALS, Volume 12, Issue 1, 2019.

[17]. Ghiban B; Antoniac I; Gheorghe D; Ghiban A; Ene R; Metallurgical failure analysis of intramedulary nail used for femoral fracture stabilization, KEY ENGINEERING MATERIALS, Volume 695, Pages 178-182, 2016.

[18]. Antoniac IV, Stoia DI, Ghiban B, Tecu C, Miculescu F, Vigaru C, Saceleanu V. Failure Analysis of a Humeral Shaft Locking Compression Plate—Surface Investigation and Simulation by Finite Element Method. Materials. 2019; 12(7):1128.

[19]. Grecu D; Antoniac I.; Trante O; Niculescu N; Lupescu O; Failure analysis of retrieved polyethylene insert in total knee replacement, MATERIALE PLASTICE, Volume 53, No.4, Pages 776-780, 2016

[20]. Bane M; Miculescu F; Blajan AI; Dinu M; Antoniac IV; Failure analysis of some retrieved orthopedic implants based on materials characterization, SOLID STATE PHENOMENA, Volume 188, Pages 114-117, 2012

[21]. ASTM E23